ENGINEERING TRIPOS PART IIA

GG2 CT Scan and Reconstruction

Interim Report

Name: Michael Hutchinson, mjh252

College: Christ's College

Contents

1 X-ray generation and scatering

CT scanning involve passing beams of *x-rays* (photons in the range 100 eV to 100 keV) through a target and measuring the intensity of the beam on the other side, usually measurd with a *scintillator* (a material that is luminescent when exposed to high energy photons). The attenuation of the beam is governed by equation 2 in the handout. The *linear attenuation coefficient* (the fraction of a beam of x-rays or gamma rays that is absorbed or scattered per unit thickness material) varies with the energy of the photons passing though it. This is dominated by the *photoelectric effect* (absorption of photons into an atom, causing electron emission) at low energies, by *Compton scattering* (interaction between a charged particle and a photon, causing the photon and particle to scatter, usually an electron) at medium energies, and by *pair production* (electron-positron creation) at high energies. Plots of these can be seen in the handout, figure 3 (left) and appendix A.1. The small jump in the photoelectric effect region is called the K-edge. In order for a photon to release an electron from an atom, it must have energy greater than that of the binding energy of the K-shell (n=1) of the atom. As the energy of a photon goes past this point, the chance of absorption jumps up, and so the linear attenuation coefficient does.

Figure 2 in the handout shows how x-ray sources are generated. Electrons fired at the spinning target undergo 2 processes to produce the distributions of x-rays seen in figure 3 (right) of the handout and A.1. First, the smooth distribution is formed by *bremsstrahlung*, or "braking energy", the excess energy released as photons as a charged particle decelerates when deflected by another charged particle. Second, the sharp peaks are called *characteristic x-rays* and are caused by electrons transitioning from higher energy shells to lower ones after vacancies are formed in the metal. This releases energy as photons. The energy gap between shells is very specific and so sharp peaks are produced. The two visible are K_α and K_β, caused by L and M shell drops respectively.

Figure 1 shows the attenuation of a real and ideal source through 2 different materials, with the log of the intensity plotted. We can see that the ideal beam forms a straight line as expected, but the real source deviates from this. This is *beam hardening* and is caused by lower energies being attenuated faster than higher energies. More examples of this for different materials can be seen in appendix A.2. The effects of this are seen later, and a partial correction applied.

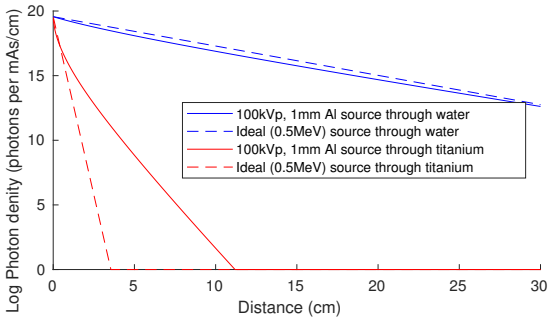

Figure 1: Comparison of different beams passing through different materials

2 CT scanning and the sinogram

In this section we look at simulating a real CT scanner in order to produce data and understand how they function. We are simulating a first generating scanner, characterised by a series of parallel beams, taken at multiple rotations about the subject. A diagram of this can be seen in the handout, figure 5, along with other generations of CT scanner.

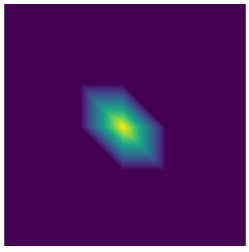

Figure 2: Zoomed in point phantom

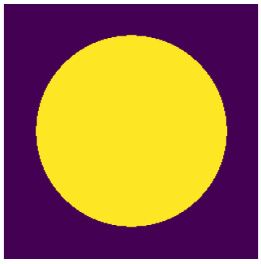

Figure 3: Disk phantom

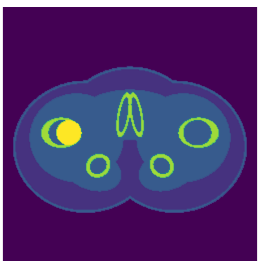

Figure 4: Pelvis with simple hip replacement phantom

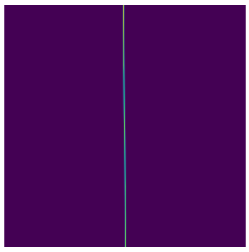

Figure 5: Sinogram of a point

Figure 6: Disk sinogram

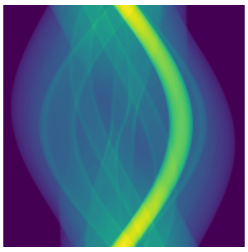

Figure 7: Pelvis with simple hip replacement sinogram

This is done by applying equation 2 from the handout along beams through the phantom, over a number of offsets, and a number of angles, to produce "sinograms" of the phantoms we are looking at. At angles where the beams do not line up with the pixels of the phantom, the depths of material were interpolated. Figures 2 to 7 show a series of phantoms and their sinograms, and more are in appendix B.1.

Investigation into the effect of different interpolation techniques of the material depths showed that either cubic (although at sharp ridges, this ran into overflow problems) or linear interpolation are useful, and that nearest neighbour interpolation is not. In regions of approximately constant attenuation coefficient we expect to see smooth sinograms, and this was given by linear and cubic, but not nearest neighbour. Images of this can be seen in appendix B.2.

Changing the number of angles scanned in a scan increases the length of the sinogram. This can be seen in appendix B.3

3 Reconstructing cross-sectional data

The next step is to reconstruct the sinograms back into phantoms. The naive way to do this is to simply smear back each line of the sinogram across the image, at the angle it was taken (equation 8 in handout). This does not work particularly well, and results can be seen in figures 8 to 10. These images are very blurry, and look like there are dominated by low frequency components.

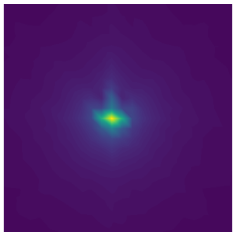

Figure 8: Unfilterd sinogram backprojction of a point

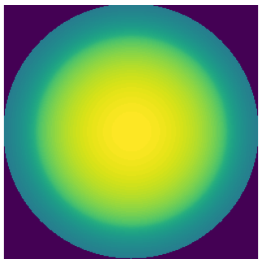

Figure 9: Unfilterd sinogram backprojction of a disk

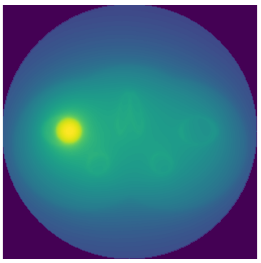

Figure 10: Unfilterd sinogram backprojction of a hip

Following the proper inversion of the radon transform from the handout and Suetens 2009 [2] we see that we must apply a filter to the sinogram data before doing back projection. The filter is the Ram-Lak filter, a symmetric ramp about 0. This fits with the results of the previous part where the image was dominated by low frequencies, as these are attenuated most. Results of applying the Ram-Lak filter to he sinogram before backprojecting can be seen in figures 11 to 13. These are clearly much better reconstructions. Figurs 12 and 13 shows clear beam hardening, with cupping and streaking. This is investigated later.

Changing the number of angles scanned has a significant impact on the quality of the reconstruction. In general, periodic noise appears on the reconstructions, radiating from places where there is a sharp change in attenuation value. This occurs as in order to represent this change, very high frequency components are required. However, the discrete number of views causes higher frequency *aliaising*, as per the Nyquist sampling theorem [1]. Appendix C.1 shows images of this (image values windowed for better viewing). At more than about 128 angles, beam hardening noise becomes more prominent than aliasing and 256+ gives a satisfactory image.

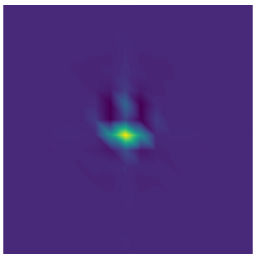

Figure 11: Filterd sinogram backprojction of a point

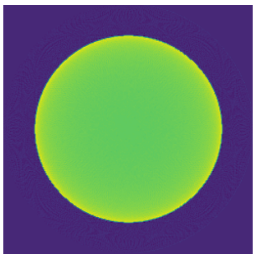

Figure 12: Filterd sinogram backprojction of a disk

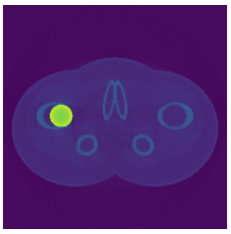

Figure 13: Filtered sinogram backprojction of a hip

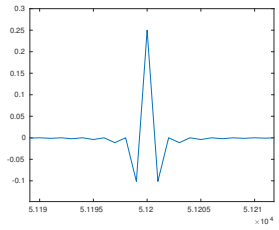

Figure 14: Ram-Lak filter impulse response

Changing the number of beams per angle also introduces aliasing noise, but in a different way. Here it appears as circles, tangential to sharp changes in attenuation coefficient. This can be seen in appendix C.2 (image values windowed for better viewing). Reducing the number of beams also reduces the resolution of the reconstruction. 256 was the minimum number of beams needed to make the beam hardening noise larger than the aliasing noise, and for a detailed enough view. 512 and above made little difference, but did produce a very low aliasing, high quality image.

Images comparing the use of different interpolation functions in backprojection can be found in appendix C.3. Linear and cubic both hid small scale noise artefacts, or reduced them well, whereas nearest neighbour did not.

The last part of this section was an investigation into how modifying the Ram-Lak filter by a cosine to a power term would affect results. Figure 9 in the handout shows what the filters would look like for different powers. From this we can see that high frequency terms have additional attenuation applied to them, and so we would expect the resulting reconstructions to be blurrier and contain fewer small details. This is clearly demonstrated in appendix C.4 where it was tested on reconstructions with poor aliasing noise. This can be a good thing as it allows us to easier see the structure in reconstruction, but the price of detail is paid, and this may be required in diagnosis. Choosing the cosine power should therefore be picked on a case basis for detail requirements.

4 Beam hardening and correction

Beam hardening is the deviation from linear attenuation of x-rays when passing through a material caused by the spread of energies in most x-ray source, and the change in linear attenuation coefficient with energy. The evolution of the energy profile of a beam passing through titanium can be seen appendix D. This leads to a non linear mapping between thickness of material and attenuation, linearity of this relationship is an assumption of the inverse radon transform. This causes 2 main artefacts: Cupping (see figure 3 and 12 for an example of this), and streaking (e.g. figure 46).

While it is difficult to correct for this across all materials, it is possible to correct for the cupping effect for a single material. This is done by measuring the thickness to attenuation relationship for a material. We then pass the sinogram through this relationship. For the chosen material, we will now have a linear mapping between depth of material and sinogram value, thus the inverse radon transform will better reconstruct the image. A more detailed treatment of this is seen in the handout. For medical purposes, water is corrected for as many materials in the body either are water, or have attenuation similar to water.

Applying this correction in the calibration step, the clear improvements can be seen in figure 15, with the disk reconstruction now being a solid disk, rather than cupped.

Figure 15: Filtered sinogram backprojction of a hip

Other methods of removing beam hardening exist. Dual energy CT scanner use 2 different energy spectrum beams to gather more information about the martial, and can remove noise hardening with this. A treatment of this can be found in Suetens 2009 [2]. Photon-counting detectors allow for the measuring of the energy of photons at the detectors, and so estimation of the energy profile of the beam. This can also be used to remove noise hardening. Finally Iterative methods such as ART allow the incorporation of prior knowledge into their reconstruction. By doing a preliminary reconstruction and identifying any high attenuation parts, the effects of these can then be simulated and this information incorporated into the next reconstruction to reduce the beam hardening artefacts they produce.

5 References

References

[1] Avinash Kak. *Principles of computerized tomographic imaging.* Society for Industrial and Applied Mathematics, Philadelphia, 2001.

[2] Paul Suetens. *Fundamentals of medical imaging.* Cambridge University Press, Cambridge New York, 2009.

[3] Henrik Turbell. *Cone-beam reconstruction using filtered backprojection.* PhD thesis, 2001.

A X-ray generation and scattering

A.1 Linear attenuation coeficients and standard x-ray sources

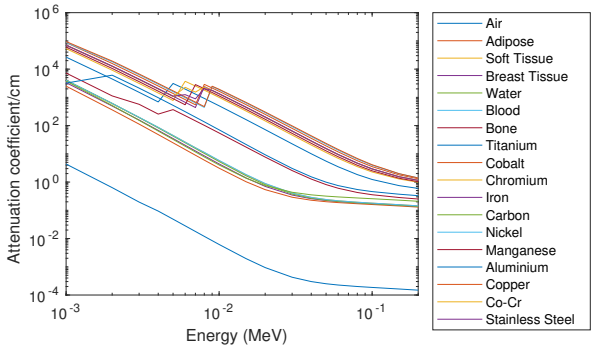

Figure 16: Linear attenuation coefficients for different materials and energies

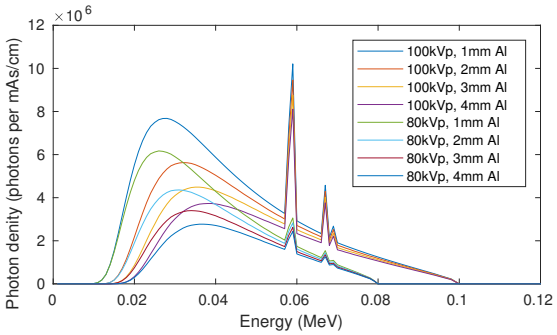

Figure 17: Photon densities for different real x-ray sources that can be used for scanning

A.2 Attenuation of beams through different materials

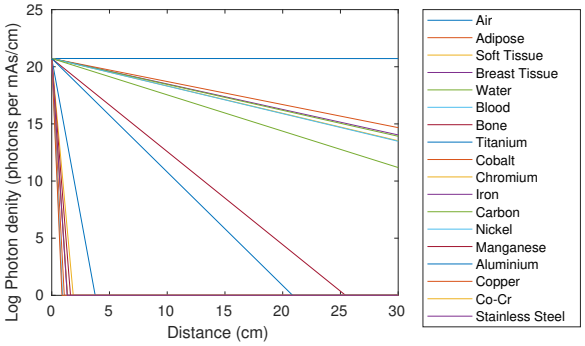

Figure 18: Attenuation of 100kVp beam, 1mm Al source through diferent materials

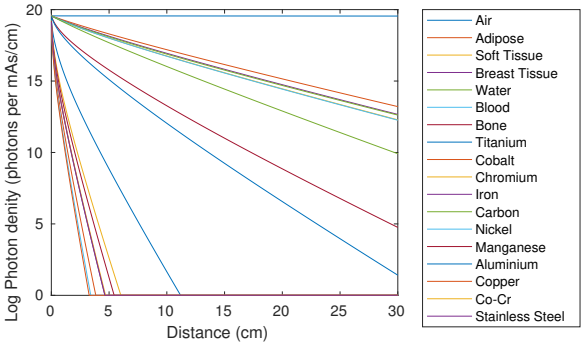

Figure 19: Attenuation of ideal source through diferent materials

B CT scanning and the sinogram

B.1 Extra phantoms and sinograms

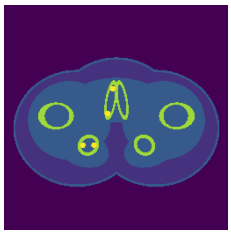

Figure 20: Pelvic pins phantom

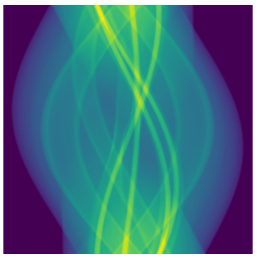

Figure 21: Pelvic pins sinogram

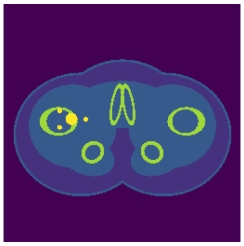

Figure 22: Sphere phantom

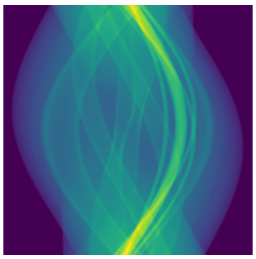

Figure 23: Sphere sinogram

B.2 Interpolation in scanning

Figure 24: Linear inperpolation in ct_scan

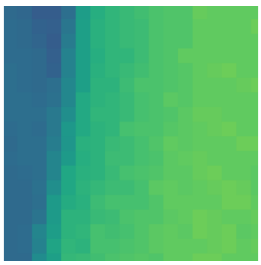

Figure 25: Nearest inperpolation in ct_scan

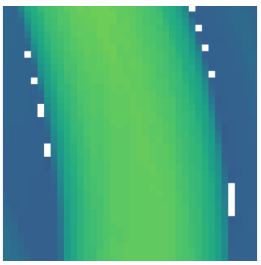

Figure 26: Cubic inperpolation in ct_scan

B.3 Investigating the number of angles scanned

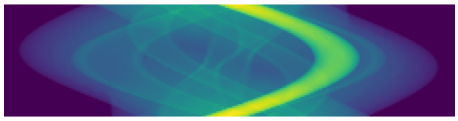

Figure 27: 64 angles

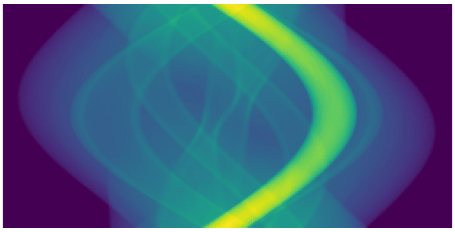

Figure 28: 128 angles

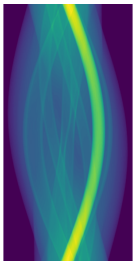

Figure 29: 512 angles

C Reconstructing cross-sectional data

C.1 Different number of angles in scans

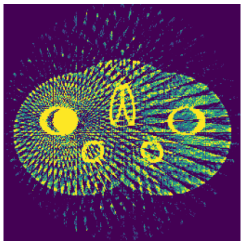

Figure 30: 32 angles in scan, 256 beams

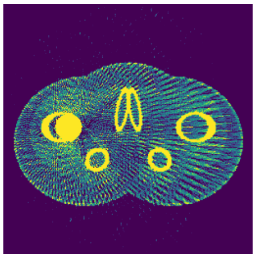

Figure 31: 64 angles in scan, 256 beams

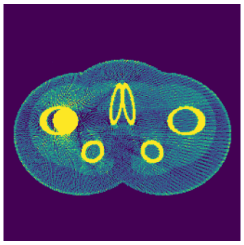

Figure 32: 128 angles in scan, 256 beams

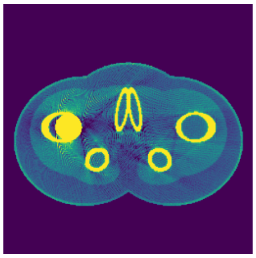

Figure 33: 512 angles in scan, 256 beams

C.2 Different number of beams in scans

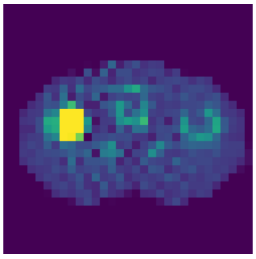

Figure 34: 256 angles in scan, 32 beams

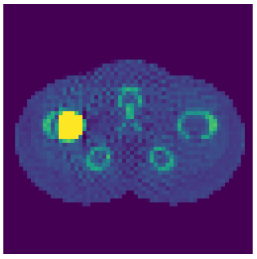

Figure 35: 256 angles in scan, 64 beams

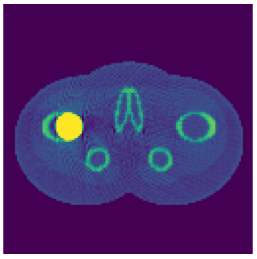

Figure 36: 256 angles in scan, 128 beams

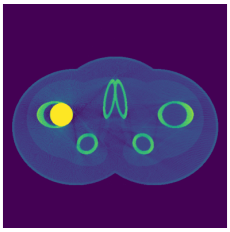

Figure 37: 256 angles in scan, 512 beams

C.3 Different interpolation functions in back projection

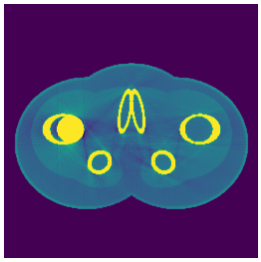

Figure 38: 256 angles in scan, 256 beams, linear interpolation

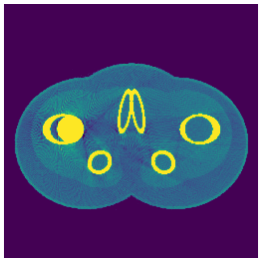

Figure 39: 256 angles in scan, 256 beams, nearest interpolation

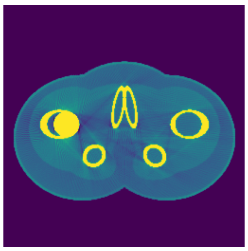

Figure 40: 256 angles in scan, 256 beams, cubic interpolation

C.4 Varying alpha in the raised cosine filter

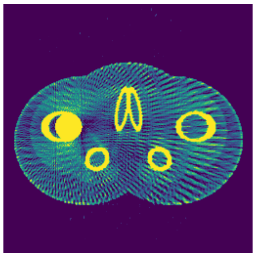

Figure 41: 256 angles in scan, 256 beams, alpha = 0.1

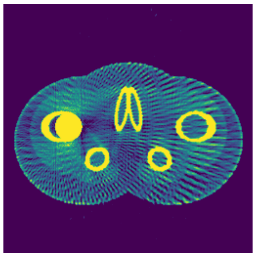

Figure 42: 256 angles in scan, 256 beams, alpha = 0.5

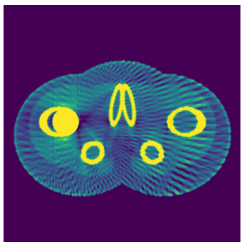

Figure 43: 256 angles in scan, 256 beams, alpha = 2

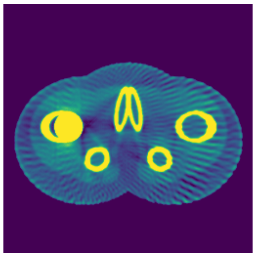

Figure 44: 256 angles in scan, 256 beams, alpha = 5

D Beam hardening and correction

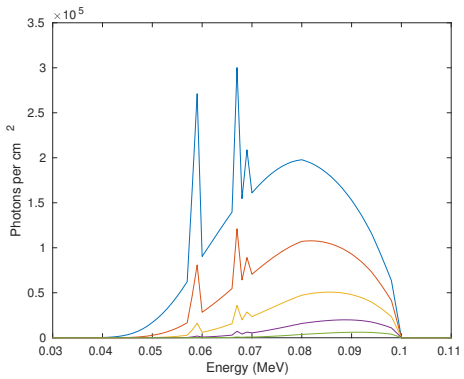

Figure 45: Evolution of a beam's energy profile as it passes through titanium

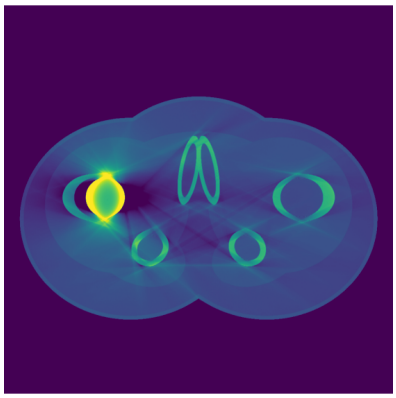

Figure 46: High beams/angles reconstruction of a hip with replacement, showing cupping beam hardening for water corrected, but streaking and titanium cupping still present.